

Supporting Information for

Offshore Crustal Thickness Variation along the Palu–Koro Strike–Slip Fault in the Sulawesi region from OBS Receiver Function Analysis

Tingwei Yang^{1,2}, ChuanChuan Lü³, Tianyao Hao^{1,2}, Nicholas Rawlinson³, Tao Xu¹, Sri Widiyantoro⁴, Alfian Alfian⁵, Muhammad Taufiq Rafie⁶, David Prambudi Sahara⁶

¹ Institute of Geology and Geophysics, Chinese Academy of Sciences, Beijing, 100029, China

² University of Chinese Academy of Sciences, Beijing 100049, China

³ Bullard Labs, Department of Earth Sciences, University of Cambridge, Cambridge CB3 0EZ, UK

⁴ Global Geophysics Research Group, Faculty of Mining and Petroleum Engineering, Institut Teknologi Bandung, Bandung, Indonesia

⁵ Seismology Exploration and Engineering Research Group, Faculty of Mining and Petroleum Engineering, Institut Teknologi Bandung, Bandung, Indonesia

⁶ Geophysical Engineering Department, Faculty of Mining and Petroleum Engineering, Institut Teknologi Bandung, Bandung, Indonesia

Correspondence to: C. Lü (chuanchuanlu@esc.cam.ac.uk)

*Corresponding authors: C. Lü (chuanchuanlu@esc.cam.ac.uk)

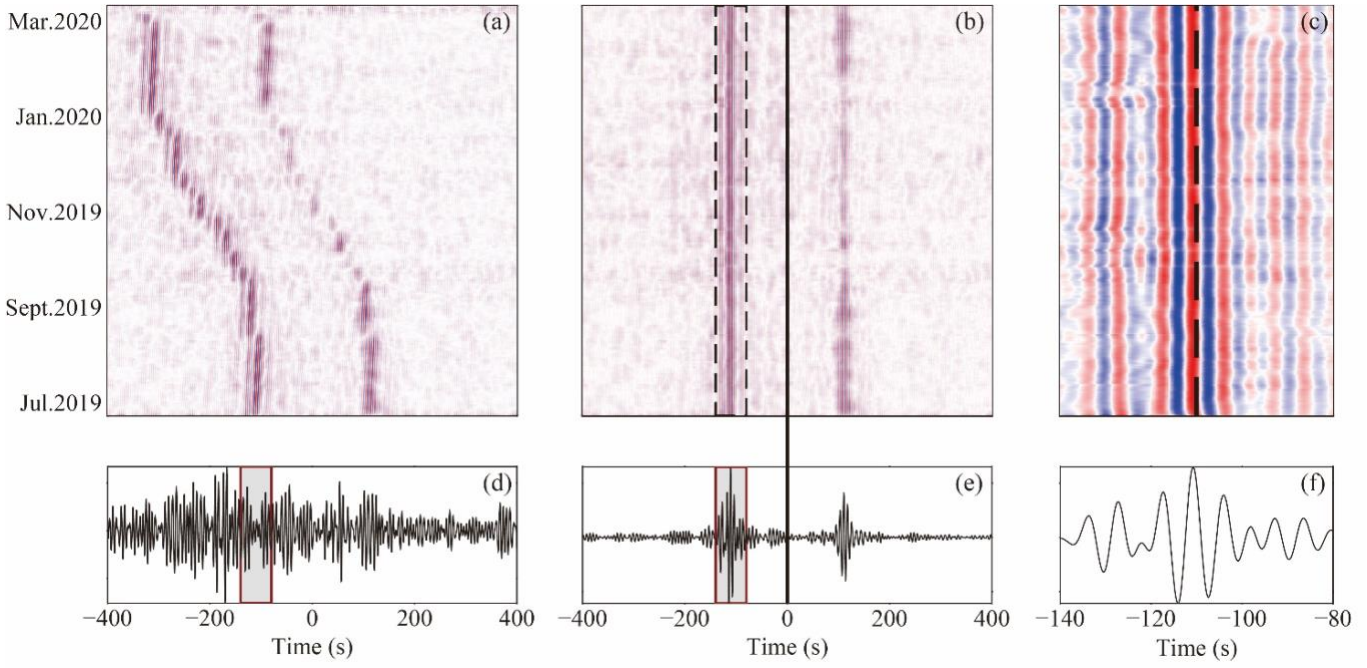
Contents of this file

Figure S1 to S12.

Supplementary Figures

Here we provide Figure. S1 showing the time correction technology proposed from the cross-correlation method of ambient noise. Figure. S2 showing the horizontal azimuth correction conducted based on minimization of tangential component of P-wave energy. And Figure. S3 showing the comparison of the OBS raw data with the preprocessed data. Figure. S4 showing the variation with time of ambient noise power spectral density at OBS and land station. Figure. S5 showing the probability density distribution of ambient noise power spectral density at OBS and land station. Figure. S6-S11 showing the receiver function waveform inversion result at OBSs. Figure. S12 showing the H- κ stacking result of OBSs.

26



27

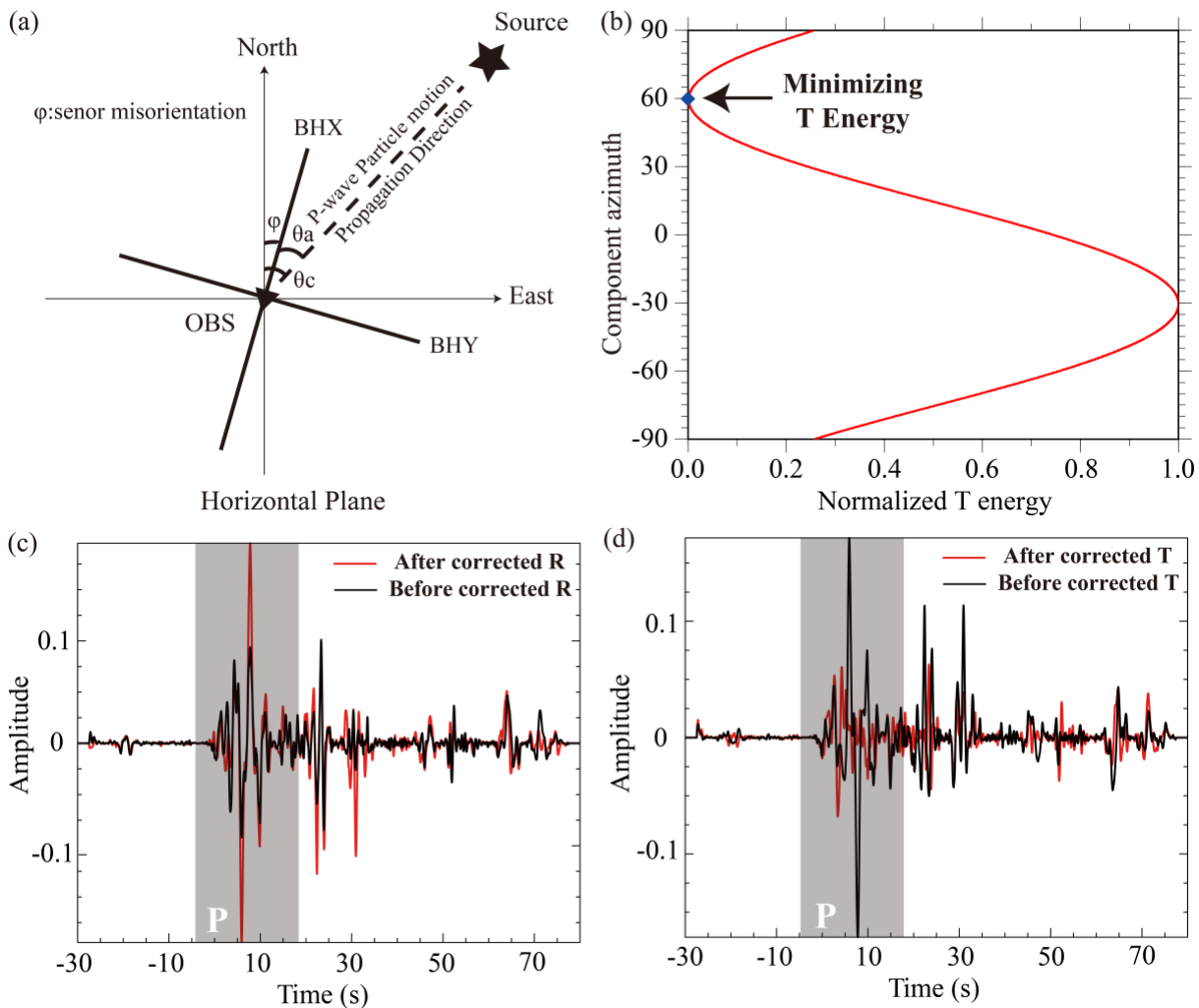
28

29

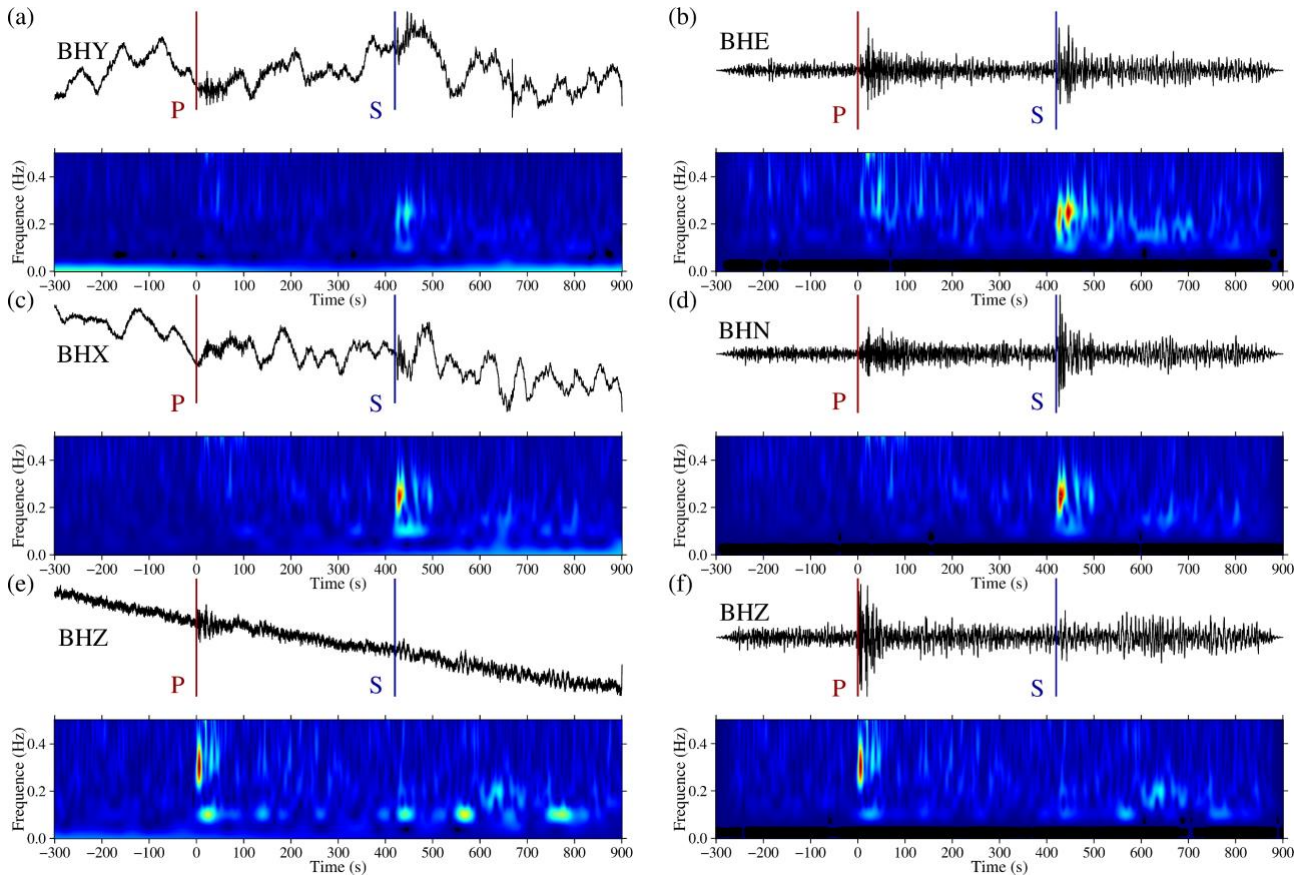
30

Figure S1: Ambient noise cross correlation functions of OBSs M01G and M02F. Raw and (b) processed ambient noise cross correlation functions arranged with time; (c) The noncausal signals of processed ambient noise cross correlation functions arranged with time; (d) Raw and (e) processed ambient noise cross correlation function after stacking; (f) Noncausal signal of processed ambient noise cross correlation functions after stacking.

31

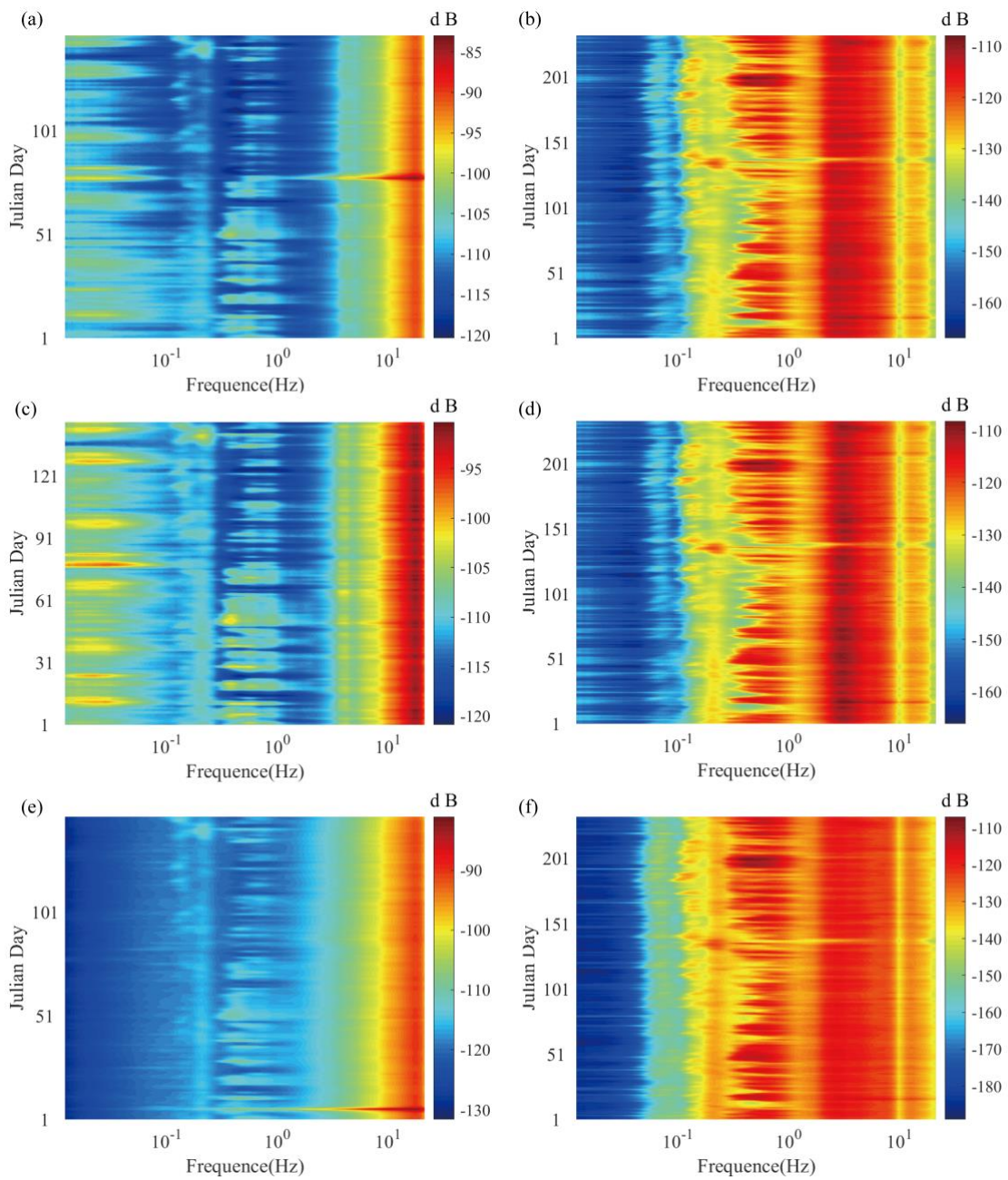


32 **Figure S2: Horizontal azimuth correction for minimizing P-wave T component energy of OBS M01G. Schematic diagram of horizontal**
 33 **azimuth deviation(φ is the clockwise azimuth deviation between the geographical North Pole and the BHX sensor; θ_c is the backazimuth**
 34 **calculated by OBS and source position geometry; θ_a is the backazimuth measured by the motion of P-wave particle); (b) Schematic search**
 35 **diagram of P-wave T component energy; Comparison of P-wave waveform of (c) R and (d) T components before and after correction.**



38 **Figure S3: Three components waveform of OBS and its results of wavelet transform. (c) and (e)are respectively indicate components BHY,**
 39 **BHX and BHZ of OBS raw data; (b), (d) and (f) are respectively indicate components BHE, BHN and BHZ of Processed OBS data.**

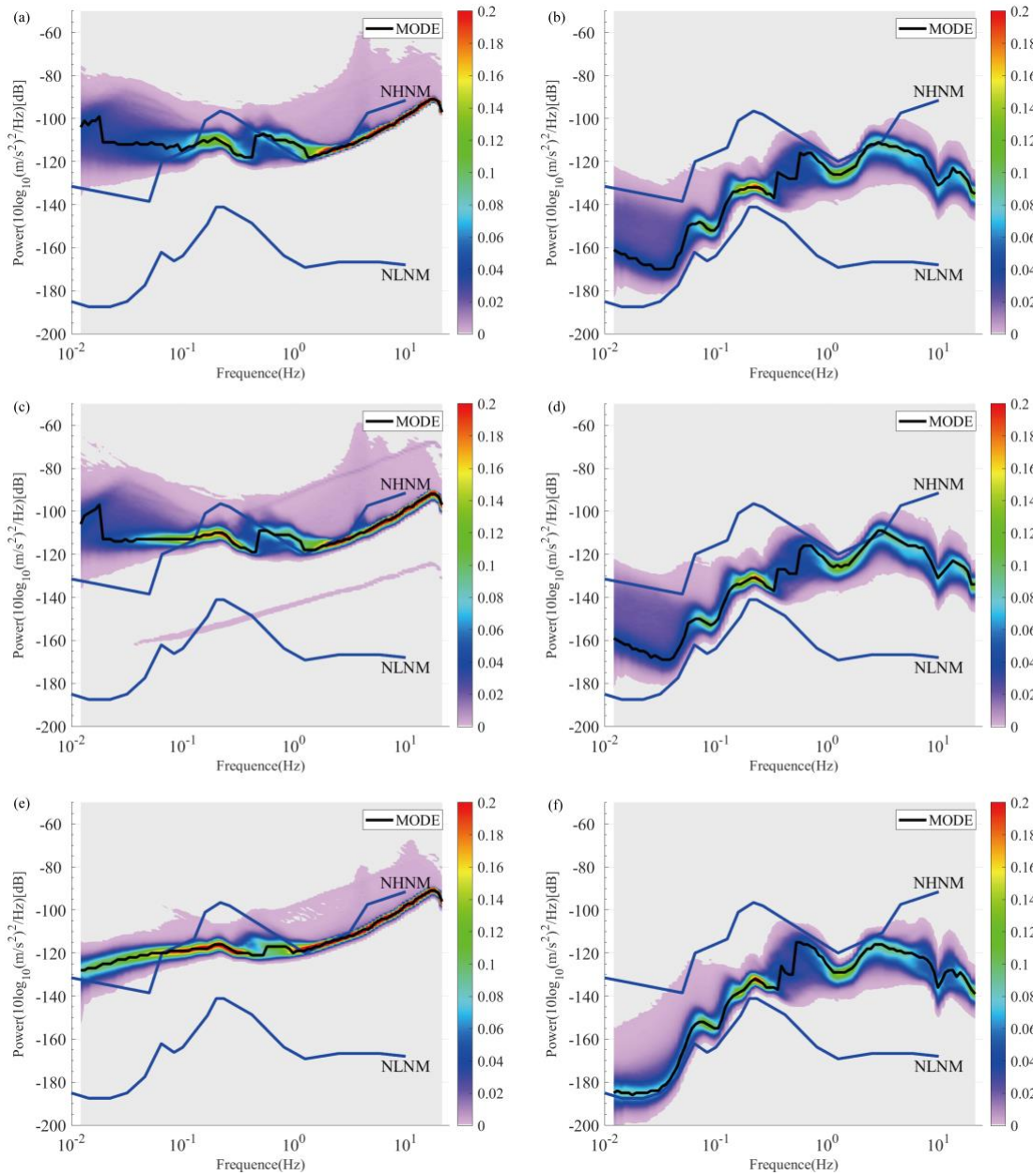
40



41

42 **Figure S4: Variation of three components ambient noise power spectral density of OBS and land station with time. (a), (c) and (e) are**
 43 **respectively indicate components BHE, BHN and BHZ of OBS M01G; (b), (d) and (f) are respectively indicate components BHE, BHN**
 44 **and BHZ of land station BKB.**

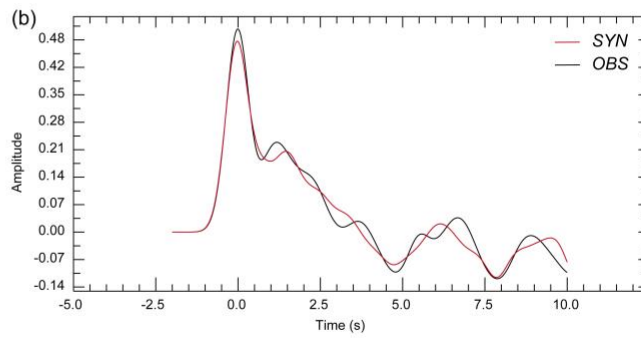
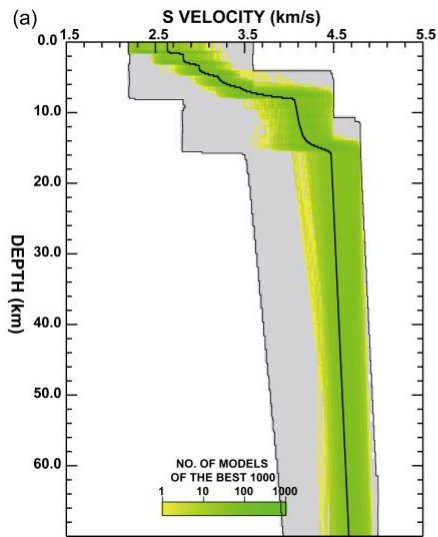
45



46

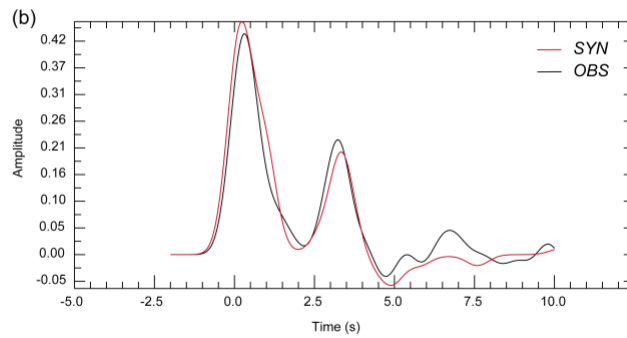
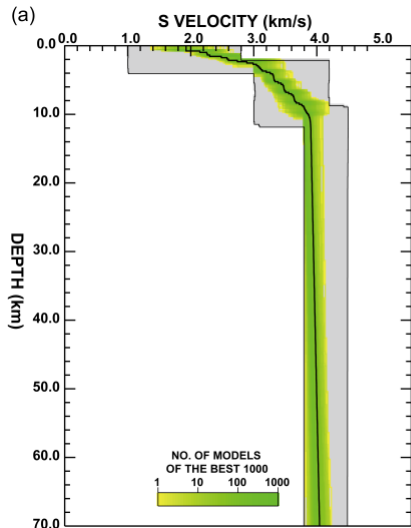
47 **Figure S5: Three components probability density distribution of ambient noise power spectral density at OBS and land station. (a), (c)**
 48 **and (e) are respectively indicate components BHE, BHN and BHZ of OBS M01G; (b), (d) and (f) are respectively indicate components**
 49 **BHE, BHN and BHZ of land station BKB.**

50



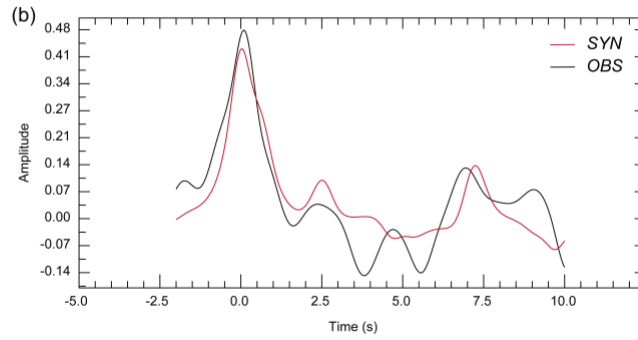
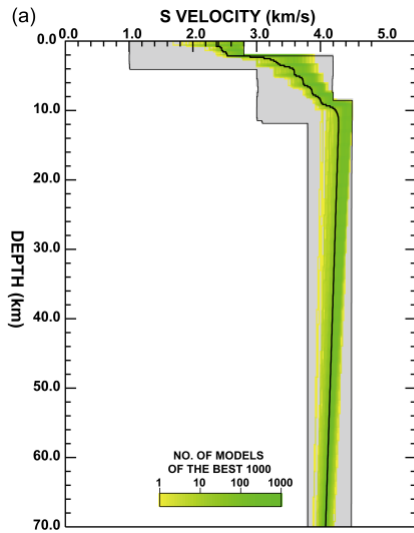
51

52 **Figure S6: Receiver function waveform inversion result at OBS site C08F. (a) The S-wave velocity structure obtained by the NA inversion**
 53 **(The thin black line encloses the search area and the black curve is the average velocity structure of the 1000 best models). (b) Receiver**
 54 **function waveform comparison (The black line is the observed receiver function and the red line is the receiver function predicted by the**
 55 **optimal model).**



56

57 **Figure S7: Receiver function waveform inversion result at OBS site C09G. (a) The S-wave velocity structure obtained by the NA inversion**
 58 **(The thin black line encloses the search area and the black curve is the average velocity structure of the 1000 best models). (b) Receiver**
 59 **function waveform comparison (The black line is the observed receiver function and the red line is the receiver function predicted by the**
 60 **optimal model).**



61

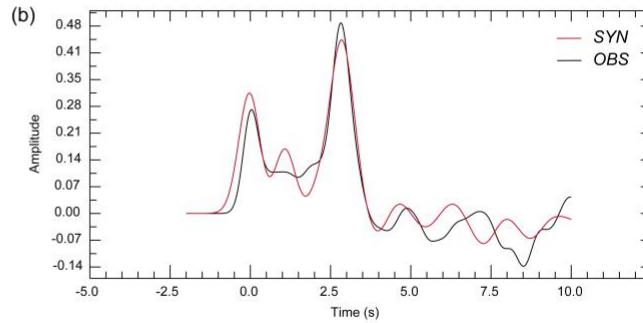
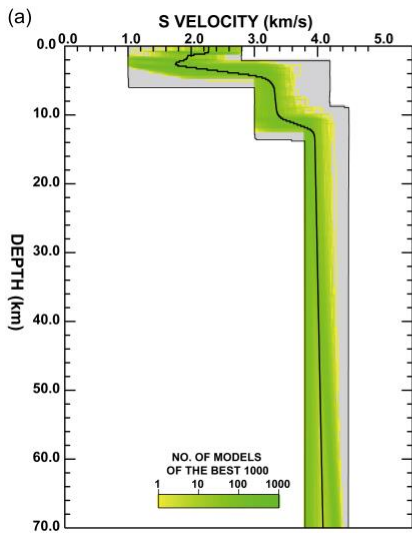
62

63

64

65

Figure S8: Receiver function waveform inversion result at OBS site C12F. The S-wave velocity structure obtained by the NA inversion (The thin black line encloses the search area and the black curve is the average velocity structure of the 1000 best models). (b) Receiver function waveform comparison (The black line is the observed receiver function and the red line is the receiver function predicted by the optimal model).



66

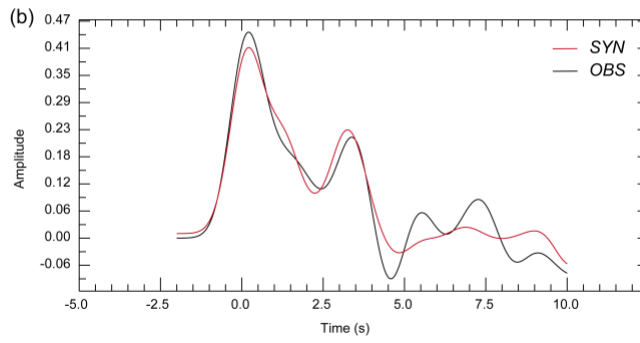
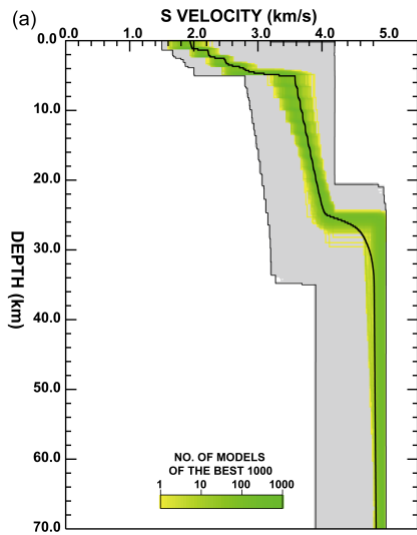
67

68

69

70

Figure S9: Receiver function waveform inversion result at OBS site C18F. The S-wave velocity structure obtained by the NA inversion (The thin black line encloses the search area and the black curve is the average velocity structure of the 1000 best models). (b) Receiver function waveform comparison (The black line is the observed receiver function and the red line is the receiver function predicted by the optimal model).



71

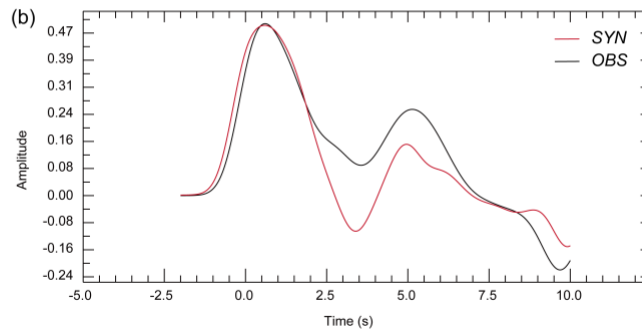
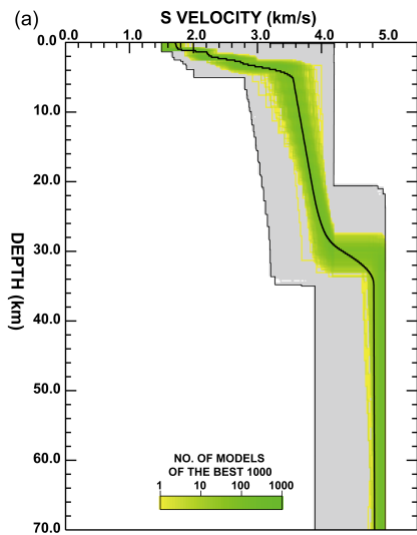
72

73

74

75

Figure S10: Receiver function waveform inversion result at OBS site M01G. (a) The S-wave velocity structure obtained by the NA inversion (The thin black line encloses the search area and the black curve is the average velocity structure of the 1000 best models). (b) Receiver function waveform comparison (The black line is the observed receiver function and the red line is the receiver function predicted by the optimal model).



76

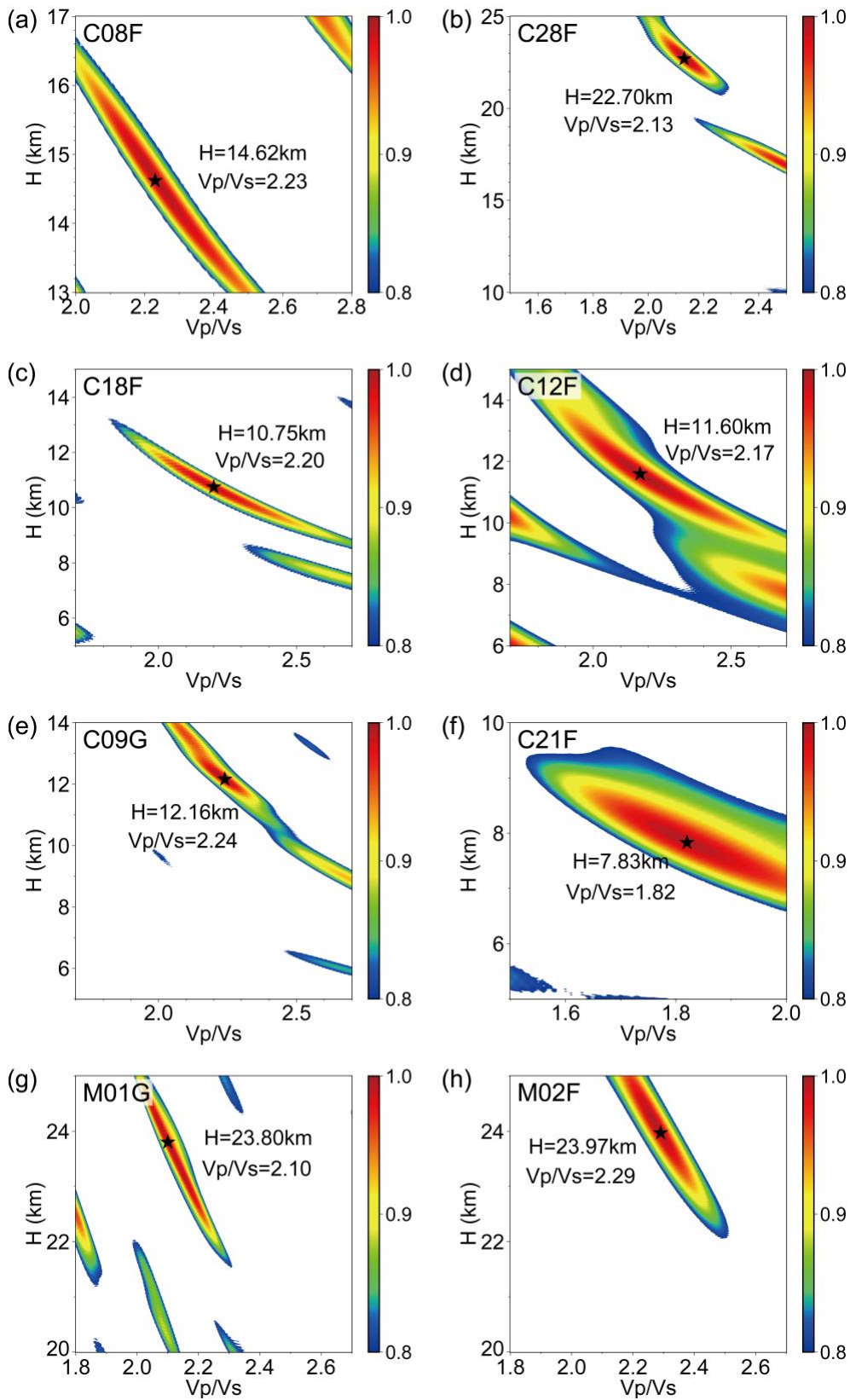
77

78

79

80

Figure S11: Receiver function waveform inversion result at OBS site M02F. (a) The S-wave velocity structure obtained by the NA inversion (The thin black line encloses the search area and the black curve is the average velocity structure of the 1000 best models). (b) Receiver function waveform comparison (The black line is the observed receiver function and the red line is the receiver function predicted by the optimal model).



81

82 Figure S12: H- κ stacking result of OBSs. The position of the five-pointed star indicates the best solution for H- κ Stacking.